ELSEVIER

Journal of Power Sources 110 (2002) 430–436

JOURNAL OF POWER SOURCES

www.elsevier.com/locate/jpowsour

# Inductive modeling of lithium-ion cells

Angel Urbina[a], Thomas L. Paez[a,*], Rudolph G. Jungst[b], Bor Yann Liaw[b]

[a]*Sandia National Laboratories, Validation and Uncertainty Quantification, 9133, Mail Stop 0557, Albuquerque, NM 87185-0557, USA*
[b]*Lithium Battery R&D Department, Sandia National Laboratories, 2521, Mail Stop 0613, Albuquerque, NM 87185-0613, USA*

**Abstract**

Sandia National Laboratories has conducted a sequence of studies on the performance of lithium ion and other types of electrochemical cells using inductive models. The objectives of some of these investigations are: (1) to develop procedures to rapidly determine performance degradation rates while these cells undergo life tests; (2) to model cell voltage and capacity in order to simulate cell output under variable load and temperature conditions; (3) to model rechargeable battery degradation under conditions of cyclic charge/discharge, and many others. Among the uses for the models are: (1) to enable efficient predictions of battery life; (2) to characterize system behavior.

Inductive models seek to characterize system behavior using experimentally or analytically obtained data in an efficient and robust framework that does not require phenomenological development. There are certain advantages to this. Among these advantages is the ability to avoid making measurements of hard to determine physical parameters or having to understand cell processes sufficiently to write mathematical functions describing their behavior. We have used artificial neural networks (ANNs) for inductive modeling, along with ancillary mathematical tools to improve their accuracy.

This paper summarizes efforts to use inductive tools for cell and battery modeling. Examples of numerical results are presented.


*Keywords:* Lithium ion; Inductive modeling; Artificial neural networks; Singular value decomposition

## 1. Introduction

Mathematical models of physical systems are constructed to facilitate our understanding of mechanisms that lead to specific responses and to enable response predictions. They are constructed in two basic frameworks: deductive (or phenomenological) and inductive (or data based).

Models are built in the phenomenological framework in most areas of science and engineering as a reflection of our desire to understand the fundamental mechanisms underlying complex phenomena. When phenomenological models can be successfully made to simulate complex phenomena, then users typically have confidence that all underlying phenomena are adequately understood and that the mathematics linking component phenomena model system behavior correctly. One potential drawback of phenomenological modeling is that it is often difficult to obtain satisfactory simulations of complex systems. There are many reasons for this. Component behaviors may not be satisfactorily modeled, and in complex systems it may not be clear how individual components influence overall response or even how collections of components interact with one another. In view of these challenges, an alternative to phenomenological modeling, such as an inductive approach might be beneficial.

Inductive models are parametric frameworks with data-based selection or training of the parameters. They usually seek to simulate excitation/response or input/output relations as interpolations among measured data, and they do so through adjustment of their parameters in a training process. Specifically, inputs that lie within the hyperspace of the training data are interpreted in terms of their neighbors and mapped into the hyperspace of outputs as an interpolation among the outputs corresponding to their neighbors. The idea behind this mapping is shown in Fig. 1.

Artificial neural networks (ANN) are frameworks that accomplish this type of mapping. We consider in this paper the use of ANNs for the inductive modeling of input/output relations in lithium-ion electrochemical cells. In particular, we model a measure of power fade in lithium-ion cells as a function of measurable cell characteristics. Some characteristics such as cell capacity can be used as measured and metrics of others may be developed. The particular ANN framework used in this investigation is the connectionist normalized linear spline (CNLS) network.

The realities of successful model construction in inductive frameworks, however, require that models be parsimonious.

* Corresponding author.
*E-mail address:* tlpaez@sandia.gov (T.L. Paez).

0378-7753/02/$ – see front matter 
PII: S0378-7753(02)00208-2

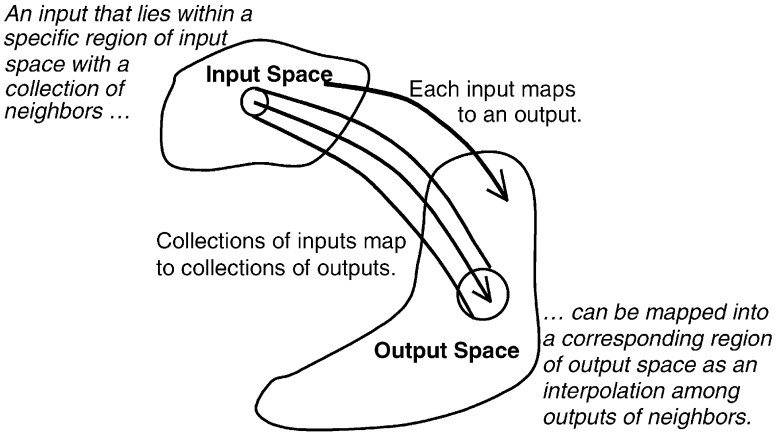


Fig. 1. Input/output mapping.

Therefore, redundancy in input information needs to be reduced as much as possible, and any successful representation needs to map inputs from a well-distributed input space to their corresponding outputs. In view of this, we also consider in this paper the use of transformations that expand measured data into well-behaved spaces. Specifically, we use the singular value decomposition (SVD) and Rosenblatt transform. A numerical example of the use of these tools to predict power fade of lithium-ion cells is presented.

## 2. Data reduction

It is often useful to express multi-dimensional quantities in a reduced space of principal components, and this is true in the current application. It is desired to express power fade in lithium-ion cells as a function of cell impedance and, possibly, other quantities. To do so efficiently in the inductive framework, the information in the impedance needs to be reduced as much as possible. There are many approaches for accomplishing this, but one that is efficient and direct is the SVD (see, for example, Golub and Van Loan [1]).

The SVD is an eigen analysis-based expansion. Its form is expressed as follows: let $\boldsymbol{x}_j, j = 1, \ldots, N$, be an ensemble of (measured) column vectors. Each vector has length $n$. In the current application these may represent complex-valued, estimated impedances of cells. Each vector element is the complex impedance of a cell at a particular frequency. Construct a matrix of the vectors following the prescription:

$$\boldsymbol{X} = \begin{bmatrix} \boldsymbol{x}_1^{\mathrm{T}} \\ \boldsymbol{x}_2^{\mathrm{T}} \\ \vdots \\ \boldsymbol{x}_N^{\mathrm{T}} \end{bmatrix} \tag{1}$$

The SVD of $\boldsymbol{X}$ has the form:

$$\boldsymbol{X} = \boldsymbol{U}\boldsymbol{W}\boldsymbol{V}^{\mathrm{T}} \tag{2}$$

The SVD is computed via eigenvalue analysis of the matrix $(\mathbf{X}^{*})^{\mathrm{T}}\,\boldsymbol{X}$. Matrices $\boldsymbol{U}$ and $\boldsymbol{V}$ have columns that are the left and right singular vectors of $\boldsymbol{X}$, respectively. $\boldsymbol{U}$ has dimension $N \times n$, and $\boldsymbol{V}$ has dimension $n \times n$. $\boldsymbol{W}$ is the matrix of singular values of $\boldsymbol{X}$. It is square with dimension $n \times n$. Each of $\boldsymbol{U}$ and $\boldsymbol{V}$ is orthonormal with respect to the identity matrix. $\boldsymbol{W}$ is diagonal and its elements are real and non-negative. The elements of $\boldsymbol{W}$ are normally arranged in descending order with the largest values at the top left, and the columns of $\boldsymbol{U}$ and $\boldsymbol{V}$ are made to correspond to this arrangement.

In terms of data expansion, the columns of $\boldsymbol{V}$ represent the principal shapes present in the $\boldsymbol{x}_j, j = 1, \ldots, N$. The components of $\boldsymbol{W}$ are the amplitudes corresponding to the shapes. Large amplitudes indicate shapes strongly represented in the data. The rows of $\boldsymbol{U}$ make the principal shapes and their amplitudes compatible with the individual row vectors in $\boldsymbol{X}$, therefore, $\boldsymbol{U}$ can be thought of as a compatibility matrix. The values in the first column are most important in characterizing the data features because they are associated with the largest singular values; the values in the second column are second most important, etc.

When the diagonal elements in $\boldsymbol{W}$ cover a wide span of magnitudes, an accurate approximate representation of $\boldsymbol{X}$ can be developed by eliminating some terms in the SVD. In particular, when all zero-valued terms and some of the smaller magnitude terms in $\boldsymbol{W}$ are eliminated along with their corresponding columns in $\boldsymbol{U}$ and $\boldsymbol{V}$, an approximation for $\boldsymbol{X}$ can be established:

$$\boldsymbol{X} = \boldsymbol{u}\boldsymbol{w}\boldsymbol{v}^{\mathrm{T}} \tag{3}$$

where $\boldsymbol{w}$ is the diagonal $m \times m$ matrix containing the $m$ largest singular values from $\boldsymbol{W}$ ($m \leq n$), and $\boldsymbol{u}$ and $\boldsymbol{v}$ are the matrices containing the first $m$ columns of $\boldsymbol{U}$ and $\boldsymbol{V}$, respectively. The matrices $\boldsymbol{u}$ and $\boldsymbol{v}$ have the dimensions $N \times m$ and $n \times m$, respectively.

The following illustrates how SVD is applied to lithium-ion battery analysis and modeling. For example, correlating impedance data among a large number of cells tested under

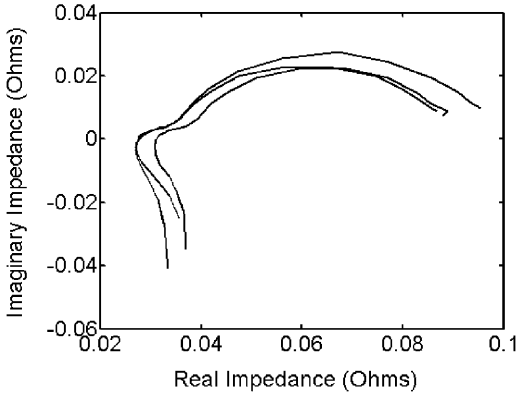


Fig. 2. Sample Nyquist plot of impedances.

various conditions is a very challenging analytical task. Consider an ensemble of 89 impedance estimates, three of which are graphed in the Nyquist plot of Fig. 2. These were obtained from 35 cells in the "new" state and following exposure to various environments. Each impedance plot is defined at 30 frequencies, and therefore, 30 complex numbers are required to completely characterize each curve. It is hoped that SVD might permit accurate, approximate characterization of a segment of the curves with fewer than 30 data points. The ohmic part of each of the 89 impedance curves was inserted as a row in $\boldsymbol{X}$ and the SVD was computed. There are 89 singular values and 10 of these are plotted in Fig. 3. The representation is clearly dominated by the first few components. Notably, for example,

$$\frac{\sum_{k=1}^{3} \boldsymbol{W}_{kk}}{\sum_{k=1}^{10} \boldsymbol{W}_{kk}} = 0.98$$

The first singular vector is graphed on the Nyquist plot of Fig. 4. This singular vector is the most important component in the ohmic part of the ensemble of the 89 impedance curves.

The first singular vector captures the great majority of the behavior of all the impedance curves. Fig. 5 is a plot of the magnitudes of the first two columns of the compatibility

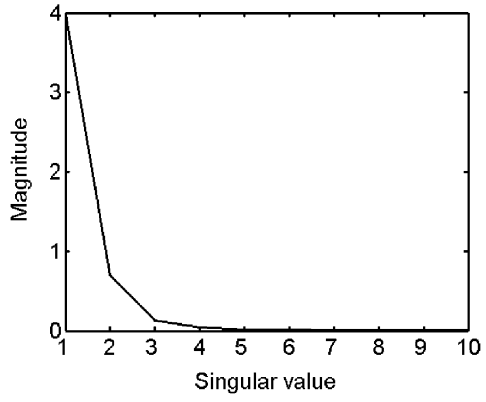


Fig. 3. Singular values, $\boldsymbol{W}$.

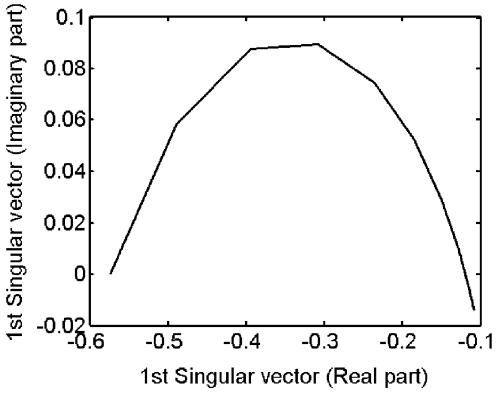


Fig. 4. Nyquist plot of the first singular vector from the ohmic part of the ensemble of 89 impedance curves.

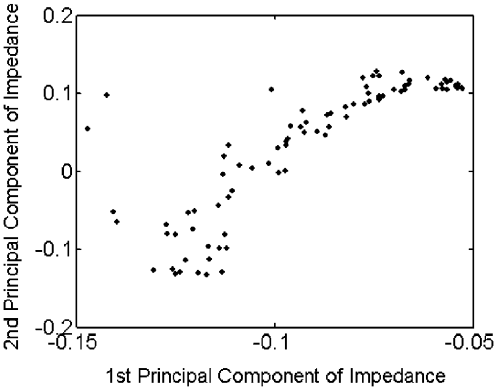


Fig. 5. Magnitude of the second column of the compatibility matrix vs. the first column of the compatibility matrix for the SVD of the impedances in Fig. 2.

matrix in Cartesian space. There are 89 data points. The abscissa value of each point (its $x$ coordinate) is the absolute value of a first column element in the compatibility matrix, $\boldsymbol{u}$. The ordinate value of the point (its $y$ coordinate) is the absolute value of the corresponding second column element of the matrix, $\boldsymbol{u}$. Three columns could be plotted in a three-dimensional space, four columns in a four-dimensional space, etc. but these are difficult to visualize. Each point in this space is a low dimensional representation of one of the 89 impedance curves in (three of which are shown in Fig. 2).

Later, the magnitude of each element in the first column of the compatibility matrix will be used as one input to an ANN whose output approximately characterizes a measure of the power fade in lithium-ion cells. The other input to the ANN will be cell capacity. Both inputs are normalized using a transformation to be discussed in the following section, before use as input to the ANN.

## 3. Data transformation

In addition to expressing the total information in all the inputs to the ANN in a minimal (or canonical) set of

variables, it is also often useful (for the sake of accuracy) to transform the inputs into a space in which they are well distributed. ANN representations are not usually good extrapolators, therefore, if the input data contains gaps or regions where the data are highly constricted, it is difficult to generate an accurate ANN mapping in these regions. For this reason, transformation of the input data into a space in which they are broadly distributed is desirable.

There are many transformations that seek to accomplish this redistribution. The most general of these is the Rosenblatt transform (Rosenblatt [2]). It transforms data (or functions) from an arbitrary space into another space with user-defined joint probability density function (PDF). In the current application we choose the transform space to be that of uncorrelated, standard normal random variables.

The Rosenblatt transform of interest to us is defined as follows. Let $F_{X_1 \ldots X_n}(x_1, \ldots, x_n)$, $-\infty < x_j < \infty, j = 1, \ldots, n$, denote the joint cumulative distribution function (CDF) of the random variables $X_j, j = 1, \ldots, n$. The Rosenblatt transform into the space of uncorrelated, standard normal random variables, $Z_j, j = 1, \ldots, n$, is defined:

$$\begin{aligned} Z_1 &= \Phi^{-1}[F_{X_1}(x_1)], \ldots, Z_n \\ &= \Phi^{-1}[F_{X_n|X_1 \ldots X_{n-1}}(x_n|x_1, \ldots, x_{n-1})] - \infty < x_j < \infty, j \\ &= 1, \ldots, n \end{aligned} \tag{4}$$

where $\Phi(\cdot)$ is the CDF of a standard normal random variable, and $\Phi^{-1}$ is its inverse, and $x_j, j = 1, \ldots, n$, are the variates corresponding to the random variables $X_j, j = 1, \ldots, n$. $F_{X_1}(x_1)$ is the marginal CDF of the random variable $X_1$, and $F_{X_n|X_1 \ldots X_{n-1}}(x_n|x_1, \ldots, x_{n-1})$ is the conditional CDF of $X_n$ given $X_1 = x_1, \ldots, X_{n-1} = x_{n-1}$. These CDFs can be obtained from the joint CDF $F_{X \ldots X_n}(x_1, \ldots, x_n)$. When joint realizations $x_j, j = 1, \ldots, n$, of the random variables $X_j, j = 1, \ldots, n$, are used on the right side of Eq. (4), they map into joint realizations $z_j, j = 1, \ldots, n$, of uncorrelated, standard normal random variables $Z_j, j = 1, \ldots, n$.

Use of the transformation defined in Eq. (4) requires approximation of the joint CDF of the $X_j, j = 1, \ldots, n$. This can be established using the kernel density estimator. Define the random vector:

$$\boldsymbol{X} = \begin{Bmatrix} X_1 \\ X_2 \\ \vdots \\ X_n \end{Bmatrix} \tag{5}$$

and let $\boldsymbol{x}_m, m = 1, \ldots, M$, be experimentally measured realizations of $\boldsymbol{X}$. Then the kernel density estimator of $\boldsymbol{X}$, an approximation to its joint PDF, is:

$$\begin{aligned} f_X(\boldsymbol{x}) &= \frac{1}{M(2\pi)^{n/2}\varepsilon^n} \sum_{m=1}^{m} \exp\left(\frac{1}{2\varepsilon^2}||\boldsymbol{x} - \boldsymbol{x}_m||^2\right), \\ &\quad -\infty < \boldsymbol{x} < \infty \end{aligned} \tag{6}$$

where $\varepsilon$ is the window width of the approximation. In applications, $\varepsilon$ can be chosen optimally using, for example, a formula given in Silverman [3]. The approximate joint CDF of $\boldsymbol{X}$ is the $n$-fold integral of Eq. (6). This can be established directly in terms of the marginal CDF of a standard normal random variable because of the absence of coupling between terms in the kernel of Eq. (6). It is:

$$\begin{aligned} F_{X_1 \ldots X_n}(\alpha_1, \ldots, \alpha_n) &= \frac{1}{M} \sum_{m=1}^{M} \prod_{j=1}^{n} \Phi\left(\frac{\alpha_j - x_{jm}}{\varepsilon}\right), \\ &\quad -\infty < \alpha_j < \infty, j = 1, \ldots, n \end{aligned} \tag{7}$$

where $x_{jm}$ is the $j$th element in the realization $\boldsymbol{x}_m$. This transformation is practically limited to random vectors of relatively low dimension because the amount of data needed to accurately form the approximations in Eqs. (6) and (7) grows as a positive constant greater than one raised to the power of the dimension $n$.

For example, consider the bivariate data plotted in Fig. 6. These are joint realizations of the magnitudes of values from the first column of the compatibility matrix of the 89 impedances (three of which are shown in Fig. 2), versus capacity values from the corresponding physical experiments on lithium-ion cells. For simplicity, we use the symbol, $\Psi$, to represent the magnitude of the first column of the compatibility matrix of the impedances (also referred to as the first principal component of the impedance). The Rosenblatt transform of the joint distribution of the random variables that yielded the data in Fig. 6 was approximated using the procedure outlined above. The data in Fig. 6 were then transformed using the representation from Eq. (7) in Eq. (4). The result is shown in Fig. 7. If the transformation were perfect, and a large amount of data were available, then the data in Fig. 7 would display radial and circumferential symmetries, generally falling within "circles" centered at the origin. However, the transformation is not perfect because the approximation in Eq. (7) is based on limited data. Still, the points in Fig. 7 are well distributed and quite

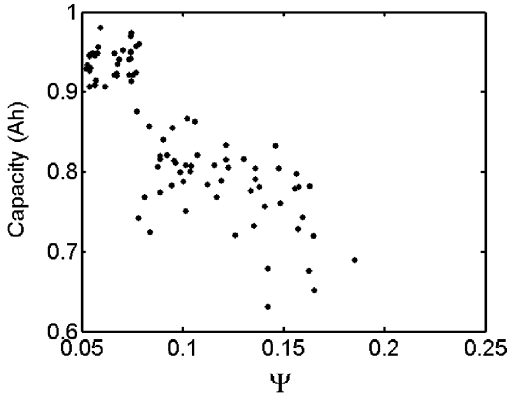


Fig. 6. Joint realizations of the magnitudes of first principal component of impedance, $\Psi$, vs. capacity values.

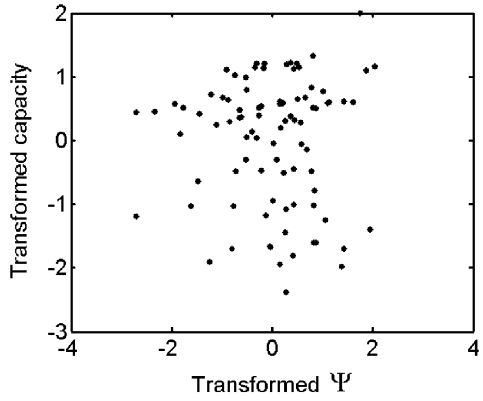


Fig. 7. Joint realizations of the magnitude of the first principal component of impedance, $\Psi$, the vs. capacity, Rosenblatt transformed into an approximately bivariate, standard normal space.

axisymmetric with no substantial gaps. They will prove useful for establishing the input to an ANN.

## 4. Artificial neural network

There are numerous ANN frameworks. The one most commonly used is the layered perceptron. It is robust and easily trainable. However, we choose, in this application, to use the CNLS network because it appears to be particularly well suited to the current application (for details see Jones, et al. [4]). This is an ANN of the radial basis function type. Its form is defined as follows. Let

$$z = g(\boldsymbol{x}) \tag{8}$$

define a deterministic mapping from the space of multivariate vectors $\boldsymbol{x}$ onto the scalar real line. Restrict $g(\cdot)$ to be continuous and to have continuous first partial derivatives in each of the variables of $\boldsymbol{x}$. The identity $g(\boldsymbol{x}) = g(\boldsymbol{x})$ can be multiplied on both sides by the radial basis function, $w(\boldsymbol{x}, \boldsymbol{c}_j, \beta)$, one of a collection of, say, $N$ radial basis functions with the same shape, and, for example, the following form:

$$w(\boldsymbol{x}, \boldsymbol{c}_j, \beta) = \exp\left(\frac{-1}{2\beta^2}||\boldsymbol{x} - \boldsymbol{c}_j||^2\right), \quad -\infty < \boldsymbol{x} < \infty \tag{9}$$

The quantity $\boldsymbol{c}_j$ is the ''center'' of the radial basis function, and $\beta > 0$ is its width. Approximate the function $g(\boldsymbol{x})$ on the right side of the resulting identity with the first two terms in its Taylor series, then sum over the set of radial basis functions to obtain:

$$g(\boldsymbol{x})\sum_{j=1}^{N} w(\boldsymbol{x}, \boldsymbol{c}_j, \beta) \cong \sum_{j=1}^{N} [g(\boldsymbol{c}_j) + (\boldsymbol{x} - \boldsymbol{c}_j)^{\mathrm{T}}\boldsymbol{D}(\boldsymbol{c}_j)]w(\boldsymbol{x}, \boldsymbol{c}_j, \beta) \tag{10}$$

where $\boldsymbol{D}(\boldsymbol{c}_j)$ is the vector of first partial derivatives of $g(\cdot)$ with respect to each variable in $\boldsymbol{x}$, evaluated at $\boldsymbol{c}_j$. Rearrange the equation and simplify variable and coefficient expressions to obtain:

$$g(\boldsymbol{x}) \cong y = \frac{\sum_{j=1}^{N} \boldsymbol{A}_j \begin{Bmatrix} 1 \\ (\boldsymbol{x} - \boldsymbol{c}_j) \end{Bmatrix} w(\boldsymbol{x}, \boldsymbol{c}_j, \beta)}{\sum_{j=1}^{N} w(\boldsymbol{x}, \boldsymbol{c}_j, \beta)}, \quad -\infty < \boldsymbol{x} < \infty \tag{11}$$

where $\boldsymbol{A}_j$ is a $1 \times (n+1)$ row vector of parameters. The parameters $A_j, j = 1, \ldots, N$, correspond to the coefficients in the Taylor series expansion of $g(\boldsymbol{x})$ at the center location $\boldsymbol{c}_j$. These are the parameters of the CNLS net and can be identified or ''trained'' using any of a number of schemes. When the training scheme permits efficient, adaptive identification of the parameters, then Eq. (11) represents an ANN.

In the current application we will normally not need to train the parameters adaptively. Rather, we will train them using weighted least squares where the weighting function is the same radial basis function that is defined in Eq. (9). Further, the sums in the numerator and denominator of Eq. (11) will not be executed over the entire set of radial basis functions. Rather, they will only be executed over those radial basis functions within some predefined distance of $\boldsymbol{x}$ (the distance is defined so that the magnitude of the radial basis functions beyond that distance are all small).

## 5. Experimental/numerical example

The combined experimental and numerical example presented here is simply a continuation of the one started in previous sections. We seek to train an ANN to simulate the input/output characteristics of some lithium-ion cell measures of behavior. Given the impedance estimate for a cell and its capacity, we seek to predict a metric of its power fade. The ANN to be trained to perform the prediction is a CNLS net. It is trained using exemplars of the two inputs. The cell capacity and the magnitude of the first column in the compatibility matrix of the SVD of the impedance curves are the two ''raw'' inputs. These are transformed into a space that is approximately uncorrelated and standard normal using the Rosenblatt transform before ANN training. The Rosenblatt transform operation was described in the section entitled ''data transformation,'' and the transformed input pairs are shown in Fig. 7.

The pulse power capability of the cell is measured by discharge and charge at 10% increments from 90 to 100% state of charge (SOC) as shown in Fig. 8. From these curves, a plot of available energy versus power can be constructed. The maximum power point occurs at zero available energy and is also shown in Fig. 8 as the crossing point between the discharge and regen pulse power capability curves. The metric used to track power fade was the power at the 300 Wh PNGV available energy requirement.

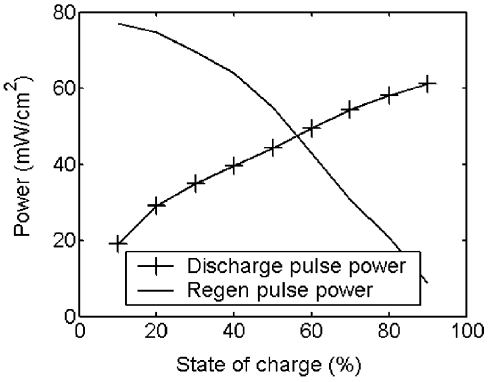


Fig. 8. Example showing the pulse capability of a lithium-ion cell defined in terms of curves established during discharge and regenerative charge of a cell at different SOCs.

A value of the pulse power capability metric is known for each bivariate input exemplar (dot) in Fig. 7. A CNLS network was trained using the estimated pulse power capability metric values (output exemplars) with the input exemplars of Fig. 7. The ANN has $N = 8$ centers. The surface generated by the trained CNLS network above a circle with radius of three units in the transformed input space is shown in Fig. 9. In addition, the training data are plotted as circles with vertical lines from the circles to the ANN surface.

Because each point in the space of transformed inputs corresponds to a bivariate quantity in the untransformed space, the result shown in Fig. 9 can also be plotted above data points in the space of capacity versus magnitude of the first column in the compatibility matrix of the SVD of impedances. This result is shown in Fig. 10.

Finally, the error of the ANN approximation at each exemplar is plotted in Fig. 11. The errors are not plotted in any particular order. The sample mean of the exemplar errors is $-0.0145$, and the sample standard deviation is 2.416. The pulse power capability values span a range of approximately 50 mW/cm$^2$. The former result leads to the conclusion that the model bias is negligible. The model standard error is approximately 5% of the span of the data.

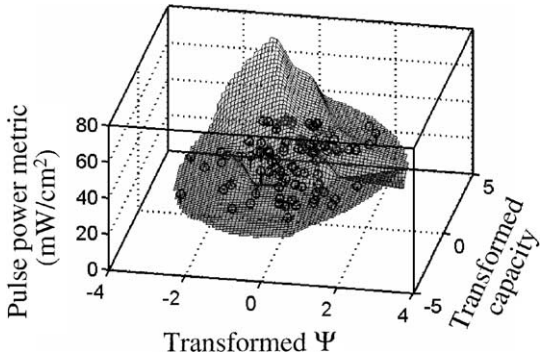


Fig. 9. Surface of trained CNLS network over the circle in the transformed input space with radius of three units, plus data (shown as o) where $\Psi$ is the magnitude of the first principal component of impedance.

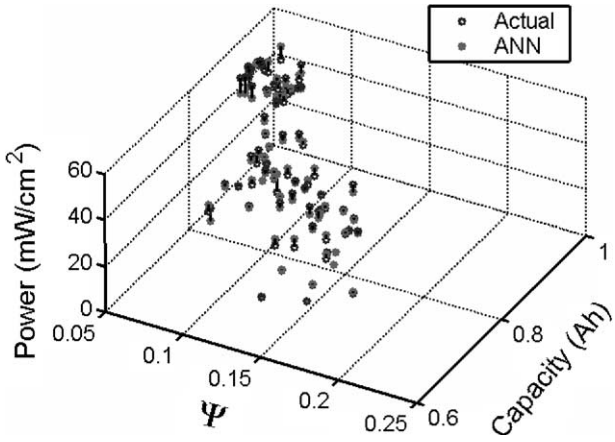


Fig. 10. Plot of the same data as shown in Fig. 9 here plotted over the untransformed input coordinates ($\Psi$ is the magnitude of the first principal component of impedance).

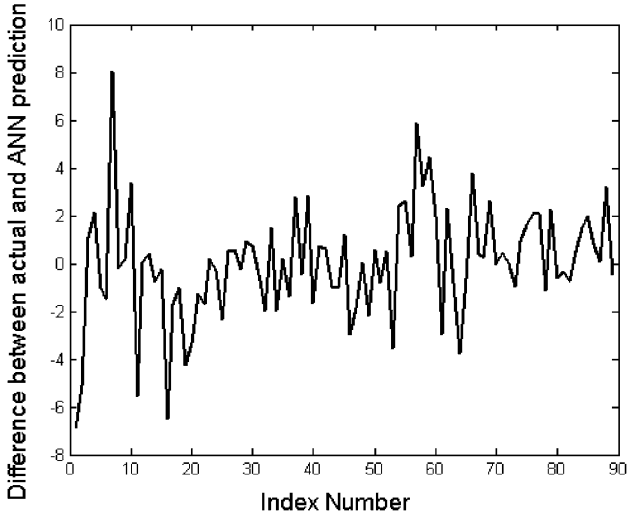


Fig. 11. ANN error.

The fact that the standard error is not smaller leads to the question: could the ANN model accuracy be improved, and if so, how? Among other things, an attempt could be made to include more raw inputs in the training data. For example, data from the second and later columns in the compatibility matrix could be used. Other measures of cell behavior might also be included as raw inputs to the ANN.

## 6. Summary

Because our primary approach for developing understanding of complex systems lies in the determination of mathematical descriptions of underlying sub-processes and the combination of these descriptions into mathematical models for the systems themselves, our goal in modeling and analysis frameworks is usually to establish comprehensive phenomenological models. However, because of the

difficulties involved in making such models accurate enough for practical use, particularly in the predictive sense, we must consider the potential for augmenting detailed phenomenological models with inductive models. ANN have the capability to transform and reduce complicated, coupled systems into an inductive framework for mathematical analysis and data-based modeling.

The study summarized here shows that at least one form of ANN, the CNLS network (and probably, many others), is capable of yielding an accurate approximation to an input/output map involving lithium-ion cell behavior measures. It was shown that the potential for creating an accurate input/output map with an ANN is improved when the input training data are transformed to eliminate (or diminish) input dependencies and when the inputs are transformed into a space where the exemplars are well distributed. Numerous methods exist for accomplishing these tasks, and the example presented in this paper is just one of them that seems promising.

The CNLS ANN was trained to represent the pulse power capability of lithium-ion cells using the inputs of cell capacity and a metric of impedance. Model bias was found to be negligible and the standard error was about 5% of the span of pulse power capability data. The accuracy of the representation could very likely be improved, and methods for exploring this possibility were discussed.

## Acknowledgements

Sandia National Laboratories is a multi-program laboratory operated by Sandia Corporation, a Lockheed Martin Company, for the United States Department of Energy under Contract DE-AC04-94AL85000. Support for this work was provided by the DOE Office of Advanced Automotive Technology through the PNGV ATD High Power Battery Program.

## References

[1] G. Golub, C. Van Loan, Matrix Computations, Johns Hopkins University Press, Baltimore, MD, 1986.
[2] M. Rosenblatt, Remarks on a multivariate transformation, Ann. Math. Stat. 23 (1952) 470–472.
[3] B. Silverman, Density Estimation for Statistics and Data Analysis, Monographs on Statistics and Applied Probability, Vol. 26, Chapman & Hall, London, 1986.
[4] R.D. Jones, et al., Cognitive Modeling in System Control, The Santa Fe Institute, 1990.